JGR Space Physics

RESEARCH ARTICLE
10.1029/2025JA033915

Observation of O+ Characteristics During the Terrestrial Alfvén Wing State Induced by the April 2023 Coronal Mass Ejection

Haoming Liang[1,2], Li-Jen Chen[2], Stephen A. Fuselier[3,4], Roman G. Gomez[3], Brandon Burkholder[2,5], Naoki Bessho[1,2], Harsha Gurram[1,2], Rachel C. Rice[1,2], Jason Shuster[6], and Akhtar S. Ardakani[6]

[1]Department of Astronomy, University of Maryland, College Park, MD, USA, [2]NASA Goddard Space Flight Center, Greenbelt, MD, USA, [3]Southwest Research Institute, San Antonio, TX, USA, [4]University of Texas at San Antonio, San Antonio, TX, USA, [5]Goddard Planetary Heliophysics Institute, University of Maryland Baltimore County, Baltimore, MD, USA, [6]Space Science Center, University of New Hampshire, Durham, NH, USA

Key Points:

- O+ ions showed field-aligned bidirectional streaming on newly-formed closed field lines (CFLs) and dominant antiparallel flux on earlier-formed CFLs
- O+ ions along with energetic protons and electrons escaped from the magnetosphere into the unshocked solar wind
- The antiparallel O+ flux reduction was associated with flux tube encounters, indicating potential loss during Alfvén wing recovery

Correspondence to:
H. Liang,
haoming@umd.edu

Citation:
Liang, H., Chen, L.-J., Fuselier, S. A., Gomez, R. G., Burkholder, B., Bessho, N., et al. (2025). Observation of O+ characteristics during the terrestrial Alfvén wing state induced by the April 2023 coronal mass ejection. *Journal of Geophysical Research: Space Physics*, *130*, e2025JA033915. https://doi.org/10.1029/2025JA033915

Received 14 MAR 2025
Accepted 9 APR 2025

Abstract We report Magnetospheric Multiscale observations of oxygen ions (O+) during a coronal mass ejection (CME) in April 2023 when the solar wind was sub-Alfvénic and Alfvén wings formed. For the first time, O+ characteristics are studied at the contact region between the unshocked solar wind and the magnetosphere. The O+ ions show energies between 100s eV and ~30 keV. The possible sources are the ring current, the warm plasma cloak, and the ionosphere. The O+ ions exhibit bi-directional streaming along newly-formed closed field lines (CFLs), and dominantly anti-parallel on earlier-formed CFLs. Escaping O+ ions in the unshocked solar wind are observed. During the recovery phase, the O+ pitch-angle distribution associated with flux tubes shows dispersion, indicating potential loss to the solar wind. Our results show escaping as well as trapped O+ ions in the region where a magnetic cloud, an Alfvén wing, and magnetospheric field lines are mixed.

Plain Language Summary During a coronal mass ejection in April 2023, NASA's Magnetospheric Multiscale mission observed oxygen ions (O+) under a rare sub-Alfvénic solar wind condition, which turned Earth's magnetic field into special magnetic structures called Alfvén wings. This study is the first to look at O+ ions in the area where the unshocked solar wind meets Earth's magnetosphere during Alfvén wing state. The O+ ions had energies from a few hundred electron volts (eV) to about 30,000 eV. These O+ ions likely came from different regions around Earth, including the ring current, the warm plasma cloak, and the ionosphere. The O+ ions moved in both directions along newly-formed closed magnetic field lines and mainly in one direction along field lines that formed earlier. Some O+ ions were observed in the solar wind, showing a dispersion pattern that suggests they might be lost to space during the recovery phase of the Alfvén wing state. Overall, the study found both escaping and trapped O+ ions in the area where the field lines of the solar wind, the Alfvén wings, and Earth's magnetosphere mix. This helps us understand how the O+ ions behave during Alfvén wing states and their potential loss to space.

1. Introduction

Understanding the interaction between the solar wind and Earth's magnetosphere is crucial in space physics. Under normal solar wind conditions, Earth's magnetosphere has regions like the bow shock, magnetosheath, and magnetopause, shaped by solar wind parameters such as Mach number, dynamic pressure, and interplanetary magnetic field (IMF) (e.g., Kivelson & Russell, 1995). Typically, the solar wind is super-Alfvénic (Alfvén Mach number $M_A \geq 8$). However, in a magnetic cloud (MC) within a coronal mass ejection (CME), the M_A can drop to 2 or less (e.g., Lavraud & Borovsky, 2008), and in rare cases, below 1, leading to Earth's Alfvén wings (e.g., Ridley, 2007). The Alfvén wings consist of open field lines connecting Earth's ionosphere and the solar corona (L.-J. Chen et al., 2024).

A low-density MC in a CME causes sub-Alfvénic flow, altering Earth's magnetosphere dynamics. Chané et al. (2012) observed Alfvén wings during sub-Alfvénic solar wind conditions on May 24–25, 2002. Chané et al. (2015) used 3D magnetohydrodynamics (MHD) model to simulate the same event, finding that the Earth's closed magnetic field line region became symmetric, extending sunward and shrinking tailward. In their case, the

open field lines underwent a change of topology aligned with the positive IMF B_y, causing field lines originating from the northern (southern) hemisphere to converge toward the dawn (dusk) Alfvén wing. They conclude that as the Alfvén wings formed, the tail lobes vanished, and auroral activity reduced significantly. Lugaz et al. (2016) used multiple spacecraft observations to study a CME on 17 January 2013, revealing a rapid and intense depletion of electrons in the outer radiation belt during the Alfvén wing state.

On 24 April 2023, a CME hit Earth's magnetosphere, observed by Magnetospheric Multiscale (MMS) in the dayside pre-noon sector near the southern cusp at (10.7, −7.9, −6.8) R_E in Geocentric Solar Ecliptic (GSE) coordinates. The MC had low density, resulting in $M_A < 1$ (by increasing the Alfvén speed). Between 12:30 and 14:40 UT, the sub-Alfvénic solar wind interacted with the magnetosphere, forming Alfvén wings (Burkholder et al., 2024; L.-J. Chen et al., 2024; Y. Chen et al., 2024).

Typically, during storm periods instigated by CMEs, O+ ions from the ionosphere are accelerated in the cusp, convected over the polar cap into the tail lobes, and then enter the plasma sheet for further acceleration and transport (e.g., Liao et al., 2015). They can be energized to a wide range of energies, from ∼10s of eV up to hundreds of keV (e.g., Fok et al., 2006). While some O+ ions return to the ionosphere, a significant portion contributes to the ring current, enhancing plasma pressure in the inner magnetosphere (e.g., Kronberg et al., 2014). During northward IMF, ionospheric O+ ions can reach the dayside magnetopause through dual-lobe reconnection (Fuselier, Trattner, et al., 2019).

The Alfvén wing state allows investigation of O+ trapping and escaping processes under extreme driving conditions, crucial for understanding of magnetosphere-ionosphere coupling. Despite previous studies, O+ behavior during the Alfvén wing state remains unclear. This study investigates O+ characteristics at the contact region between the unshocked solar wind and the magnetosphere for the first time. We use MMS observations (Burch et al., 2016) in the magnetic cloud, an Alfvén wing, and the freshly-formed closed field line (CFL) region during the CME event on 24 April 2023. This CFL region results from dual-wing reconnection (L.-J. Chen et al., 2024; Gurram et al., 2024), similar to dual-lobe reconnection under super-Alfvénic solar wind with northward IMF. This study illuminates the impact of Alfvén wings on O+ circulation in Earth's magnetosphere and provides insight into heavy ion circulation during the Alfvén wing state for extrasolar planets (Saur et al., 2013) and planetary satellites (Kivelson et al., 2004; Neubauer, 1998). While single-point observations limit our ability to determine global O+ transport and energization mechanisms, this work offers valuable insights into O+ behavior under the rare conditions and serve as constraints and validation points for models reconstructing the O+ transport and energization during sub-Alfvénic solar wind conditions.

2. Methodology

We use magnetic field data from the Fluxgate Magnetometer (FGM) (Russell et al., 2014), electron and ion data from the Fast Plasma Investigation (FPI) (Pollock et al., 2016), energetic electron data from the Fly's Eye Energetic Particle Spectrometer (Blake et al., 2016), and H+ and O+ data from Hot Plasma Composition Analyzer (HPCA) (Young et al., 2016). In this work, the bleedover of intense proton (H+) fluxes leads to contaminated O+ flux (Fuselier et al., 2021). Based on time-of-flight data between 14:05 and 14:25 (not shown), the O+ flux below 10-keV was contaminated. While genuine O+ signals could exist below this energy level, to ensure reliability, we use the 10-keV as the conservative threshold for uncontaminated O+ signals. The O+ contamination below 10 keV from 12:30 to 14:24 UT and from 14:38 to 16:18 UT, and below 300 eV from 16:18 to 16:23 UT, was removed before plotting the moments and spectra.

3. Results

3.1. Overview

The primary focus here is to report O+ ion characteristics of trapping and escaping in the region with a mixture of a MC, an Alfvén wing, and magnetospheric field lines (14:00–14:40 UT), and in the region with isolated flux tubes in the shocked solar wind (15:00–15:22 UT) immediately after the Alfvén wing phase.

Figure 1 provides an overview of this event, including O+ observations (Figure 1e). After 12:30 UT, MMS observed only the unshocked solar wind until 14:05 UT (Figure 1g). According to L.-J. Chen et al. (2024), from 14:05 to 14:38 UT, MMS observed Alfvén wing filaments. They were identified by energized electrons and ions with no significant enhancement in the upstream solar wind, suggesting the particles probably originated from

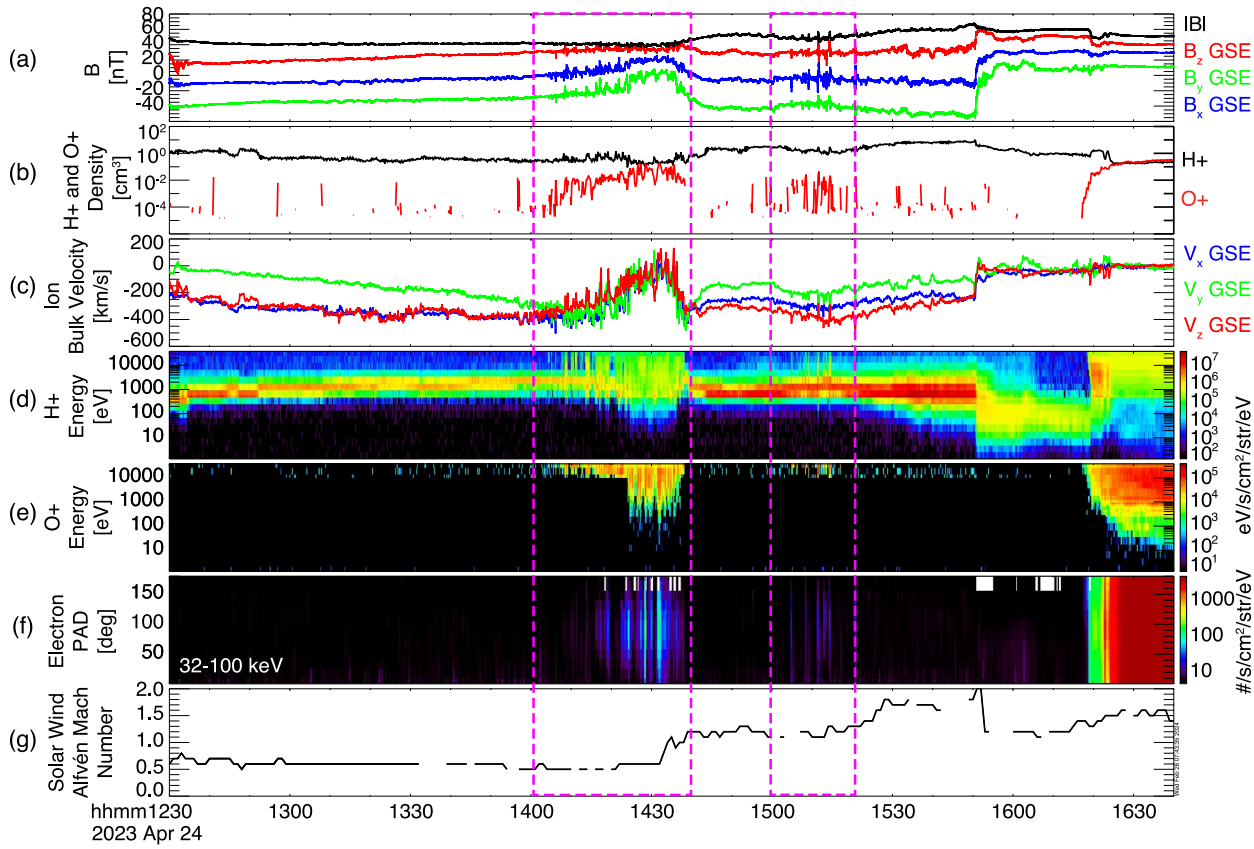

Figure 1. Overview O+ observations in the 2023 April coronal mass ejection event: (a) magnetic field, (b) H+ and O+ densities, (c) ion bulk velocity, (d) H+ energy flux, (e) O+ energy flux, (f) electron pitch-angle distribution for 32–100 keV, and (g) the Alfvén Mach number M_A from the OMNI data set using Wind as the upstream spacecraft. Highlighted intervals are discussed in detail in this work.

Earth or were generated by magnetic reconnection. The energetic electron pitch-angle distribution (PAD) (Figure 1f) and the hot ions (Figure 1d) provide evidence of CFLs. A primary CFL region was also captured between 14:25 and 14:35 UT. According to L.-J. Chen et al. (2024) and Gurram et al. (2024), this region was found to be freshly formed likely due to dual-wing reconnection. Although it differs from the magnetospheric steady CFL region at 16:30 UT, the magnetic field components and ion densities were similar to those at 16:30 UT.

Before the sub-Alfvénic solar wind ended locally at MMS around 14:40 UT (L.-J. Chen et al., 2024), the O+ density and flux were enhanced (Figures 1b and 1e) between 14:05 and 14:38 UT. This enhancement occurred during the Alfvén wing state, with O+ flux observed on both open and CFLs.

After ∼14:40 UT, the solar wind became super-Alfvénic (M_A = 1.1–2.0) (Figure 1g), causing the dayside magnetopause to move away from MMS. From 15:00 to 15:22 UT, MMS observed isolated flux tubes with O+ enhancements during this recovery phase from the Alfvén wing state.

In the following sections, we analyze the O+ characteristics in the highlighted intervals in Figure 1. From 14:00 to 14:40 UT, O+ characteristics were observed in the region with mixed field lines of the MC, Alfvén wing, and magnetosphere during the Alfvén wing state. From 15:00 to 15:22 UT, O+ behavior was observed associated with isolated flux tubes during the recovery phase.

3.2. O+ Trapping and Loss During the Alfvén Wing State (Interval 14:00-14:40 UT)

Figure 2 show observations from 14:00 to 14:40 UT during the interaction between the unshocked solar wind and the magnetosphere. The O+ density (Panel a) increases as the H+ perpendicular bulk speed (Panel b) decreases from ∼600 km/s at 14:00 UT to ∼200 km/s around 14:25 UT. The 20eV–20 keV electron energy fluxes parallel

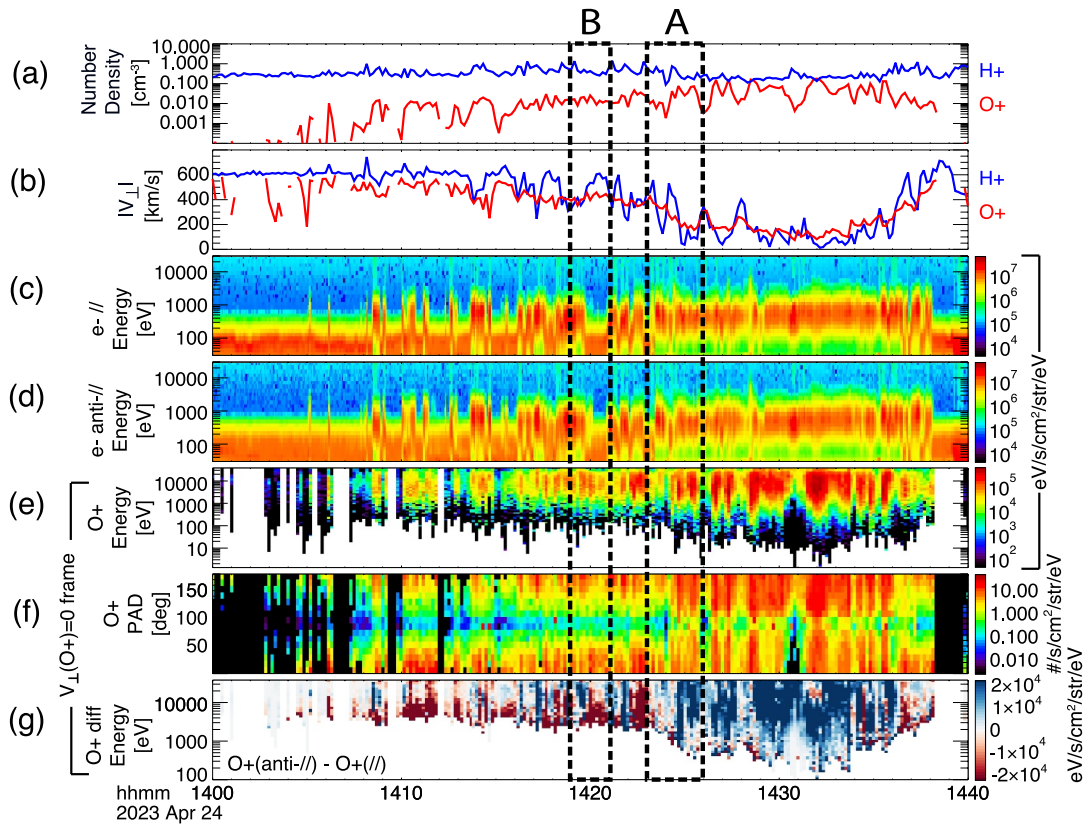

Figure 2. Observations between 14:00 and 14:40 UT (a–g) and between 14:23 and 14:26 UT (h–m): (a) H+ and O+ number density, (b) magnitudes of H+ and O+ bulk velocities perpendicular to the local magnetic field, (c) parallel and (d) anti-parallel field-aligned electron energy flux, (e) O+ omni energy flux (f) O+ PAD (g) anti-parallel O+ energy flux (120°–180°) subtracted by parallel energy flux (0°–60°). (e–g) are in the $V_{\perp}(O+) = 0$ frame. Black dashed boxes highlight the Intervals A and B for zoom-in view.

(Panel c) and anti-parallel (Panel d) to the local magnetic field distinguish field line connectivity (e.g., Burkholder et al., 2022; Fuselier et al., 2022, 1997). Detailed analysis in L.-J. Chen et al. (2024) shows that the Alfvén wing filaments, newly-formed CFLs due to dual-wing reconnection, and MC field lines, are intermittently observed from 14:05 to 14:24 and 14:37 to 14:38 UT, while a primarily magnetospheric CFL region is observed from 14:25 to 14:35 UT. The Alfvén wing filaments are generated by reconnection between the MC field lines and the CFLs north or south of the MMS.

O+ ions typically indicate connection to Earth's magnetic field lines; however, on the spatiotemporal scales of transient structures smaller than the O+ gyro-motion, they may also be observed on the MC field lines. Between 14:05 and 14:24 UT, the O+ flow was separated from the H+ flow (Figure 2b). One possible explanation is different sources and physical processes they experienced while escaping from the magnetosphere (e.g., Fuselier et al., 1995; Fuselier, 2020; Möbius et al., 1986). The observed H+ included both solar wind and magnetosphere origins, while the O+ ions were from the magnetosphere.

Given the significant O+ perpendicular flow variation (200–500 km/s), we analyze the O+ characteristics in a frame where its perpendicular bulk velocity is zero (i.e., $V_{\perp}(O+) = 0$ frame) (Fuselier, Mukherjee, et al., 2019). This involves calculating the bulk velocity from the O+ velocity distribution function (VDF), determining the perpendicular component to the local magnetic field, and shifting the VDF origin by the perpendicular bulk velocity. This transformation removes perpendicular drift motions, facilitating analysis of thermal and field-aligned motions. Limitations may arise in regions with rapid changes of the local magnetic field direction. We assume no significant variations within the 10-s cadences of the HPCA data when calculating the perpendicular bulk velocities. For the scales and phenomena examined in this study, this condition is met, providing valuable insights into O+ dynamics.

We transform the O+ energy spectra and PAD to the $V_\perp(O+) = 0$ frame (similar to the $V_\perp(H+) = 0$ frame in Fuselier, Mukherjee, et al. (2019)), as shown in Figures 2e and 2f, respectively. The O+ energy in the $V_\perp(O+) = 0$ frame ranges from 1 to 30 keV (Panel e), consistent with the combined warm plasma cloak (up to a few keV) (Chappell et al., 2008) and ring current populations. The observed O+ population may also include energized O+ by reconnection north or south of the spacecraft along the field lines.

Although the O+ PAD shows bidirectional field-aligned distributions, the fluxes between parallel and anti-parallel are asymmetric on most open and CFLs. The asymmetry can result from different sources or gradual loss of the populations. The newly open Alfvén wing filament field lines due to reconnection (L.-J. Chen et al., 2024) can gradually lose O+ along the field lines. The timescale of trapped O+ loss is proportional to the bouncing period before the CFLs open. For a 10-keV O+ ion with a 30-degree pitch angle at the equatorial plane $L = 10$, the bouncing period between the northern and southern mirror points of is about 12 min (Jordanova et al., 2020). Therefore, an O+ ion at the equatorial plane reaches one mirror point in 3 min (6 min if starting from the opposite hemisphere's cusp region). This estimate provides the timescale for O+ loss on a newly open field line. Since the Alfvén wing filament intervals are shorter than the O+ escaping time, it is reasonable that MMS still observes the counter-streaming O+ PAD (similar to trapped O+ signatures) on the Alfvén wing filaments between 14:05 and 14:24 UT (Figure 2f).

The O+ energy spectrum and PAD between 14:25 and 14:35 UT may indicate multiple O+ sources. In this interval, $V_\perp(O+) = V_\perp(H+) = 0$, and CFLs are dominant (L.-J. Chen et al., 2024; Gurram et al., 2024). The lower limit of the O+ energy in the $V_\perp(O+) = 0$ frame dropped to ~100 eV, significantly lower than that in the convecting magnetic structures between 14:05 and 14:24 UT. The warm plasma cloak and ionospheric O+ outflow may contribute to the low energy population (<1 keV). The O+ PAD between 14:25 and 14:35 UT shows counter-streaming signatures with broader pitch-angle ranges than those observed between 14:05 and 14:24 UT. The observed lower limit of O+ energy (~100 eV) is higher than that in the regions with the steady magnetospheric CFLs at 16:30 UT (~20 eV) (Figure 1e).

We compare O+ flux between 14:05–14:24 UT and 14:25–14:35 UT. Figure 2g shows the difference between anti-parallel and parallel O+ energy flux (anti-parallel minus parallel), where the parallel and anti-parallel are integrated over pitch-angles 0°–60° and 120°–180°, respectively. The selection of pitch-angle range is based on the O+ PAD enhancement between 14:05 and 14:24 UT. Positive values (blue) indicate dominant anti-parallel flux, suggesting net O+ flow from north to south along the field lines. Negative values (red) indicate dominant parallel flux, suggesting net O+ flow from south to north. This representation visualizes the energy-dependent flow directions of O+ populations inside the CFLs. Figure 2g shows a mixture of parallel and anti-parallel flux between 14:05 and 14:24 UT and a dominant anti-parallel O+ flux between 14:25 and 14:35 UT. We investigate the O+ characteristics in Intervals A and B for deeper insights.

To examine the O+ characteristics on the CFLs, we focus on Interval A (14:23–14:26 UT) as shown in Figure 3. According to L.-J. Chen et al. (2024), Interval A marks the entry into the CFL region. Selected intervals are highlighted by red and blue dashed boxes. The ion energy spectrum (Panel a) shows varying states of deceleration and heating. These variations depend on the time elapsed since CFL formation. In the blue boxes, ions are fully heated, indicating earlier CFL formation. In the red boxes, a cold ion beam (similar to the MC-like population in 14:23:00–10 UT but decelerated) with a heated background suggests newly-formed CFLs. Panel b shows less intense O+ energy flux on the newly-formed CFLs than on the earlier-formed ones. Panel d shows a mixture of parallel and anti-parallel fluxes at various energy channels on the newly-formed CFLs, indicating the O+ sources at the north and south of MMS.

The 10-s cadence of the O+ data, a limitation of the HPCA instrument, is needed to accumulate sufficient counts for a full O+ distribution function. This cadence is longer than the intervals of transient structures, for example, Alfvén wing filaments and newly-formed CFLs, potentially causing temporal aliasing where parallel and anti-parallel O+ fluxes may occur at different times within intervals shorter than 10 s.

For the earlier-formed CFLs, the O+ flux is mainly anti-parallel, indicating the O+ population originates north of the MMS. The O+ ions propagated to the observed CFL regions along the field lines. The O+ ions with pitch angles near the parallel or anti-parallel directions propagated faster than those with near-perpendicular pitch angles. Consequently, we observed mainly parallel (0°–60°) and anti-parallel (120°–180°) O+ fluxes on the newly-formed CFLs, while the earlier-formed CFLs exhibited relatively more O+ fluxes with near-perpendicular

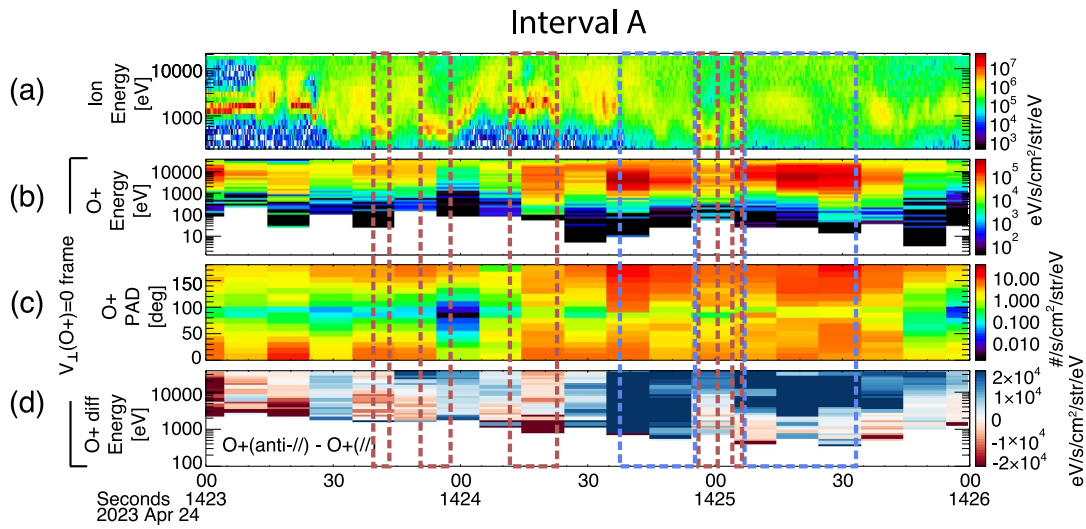

Figure 3. Observations in the Interval A (14:23–14:26 UT) from Figure 2: (a) ion energy spectrum, (b) O+ omni energy flux (c) O+ PAD (d) anti-parallel O+ energy flux (120°–180°) subtracted by parallel energy flux (0°–60°). (b–d) are in the $V_{\perp}(O+) = 0$ frame. Red (blue) dashed boxes highlight the intervals with newly-formed (earlier-formed) closed field lines.

pitch angles (Figure 3c). The O+ PAD features may allow us to estimate the time since these two types of CFLs formed by assuming the O+ were trapped in a perfect dipole field. However, this assumption is invalid. Firstly, the solar wind dynamic pressure increases the field strength at low latitudes and causes deviations from a dipole field. In addition, the CFLs were formed due to dual-wing reconnection, and their orientation aligned with the IMF with a dominant B_y component, which further deviated from a dipole field configuration. Therefore, finding a quantitative correlation between the O+ PAD and the formation timescales for these CFLs needs more information.

Escaping O+ in the unshocked solar wind was observed in Interval B (14:19–14:21 UT) in Figure 4, highlighted by the magenta box. Panel a shows the cold ion beam (~1–2 keV) as the MC population, while the energetic ion population (6–20 keV) likely originates from the magnetosphere. The ion spectra (Panels b–d) display two transient parallel flux bursts at 14:20:22 UT and 14:20:34 UT superimposed on a perpendicular flux background. Panel e reveals two energetic parallel electron jets (32–100 keV) at 14:20:15 UT and 14:20:35 UT. These particle parallel flux bursts indicate enhanced magnetic connectivity between the magnetospheric source region and our observation site, analogous to the field-aligned electron, proton, and O+ ions escapes observed during radial IMF configurations by Möbius et al. (1986). A bidirectional O+ flux with dominant parallel flux (2–20 keV) is seen in Panels f–h. These escaping O+ signatures, along with energetic protons and electrons, resemble observations in the magnetosheath during super-Alfvénic solar wind by Möbius et al. (1986). Although the energies of the escaping species in our study are lower than those in Möbius et al. (1986) (≥40 keV for ions, 70–207 keV for electrons), this observation updates our knowledge of escaping O+ energy. This suggests an O+ escape path with less energization compared to typical super-Alfvénic solar wind conditions. The fate of the escaping O+ remains uncertain; they may either propagate with the MC or return to the magnetosphere due to their large gyro-radius and the near-tangential configuration of the MC field lines to the magnetosphere.

3.3. O+ Loss During Alfvén Wing Recovery (Interval 15:00-15:22 UT)

Multiple isolated flux tubes were observed between 15:00 and 15:22 UT (marked by the magenta arrows in Figure 5d1). During this interval, the solar wind became super-Alfvénic (M_A = 1.1–2.0) and the magnetosphere contracted (dayside magnetopause moved inward).

The ion speed was about 500 km/s (Figure 5b1). We analyze O+ behavior in the frame where ion perpendicular velocity is zero ($V_{\perp}(H+) = 0$), as this frame represents the convection of the isolated flux tubes with embedded O+ ions. Here, the $V_{\perp}(H+)$ is calculated using FPI ion bulk velocity. The O+ energy in the $V_{\perp}(H+) = 0$ frame was above ~1 keV (Panel h1). Although the O+ population in these flux tubes was likely the magnetospheric

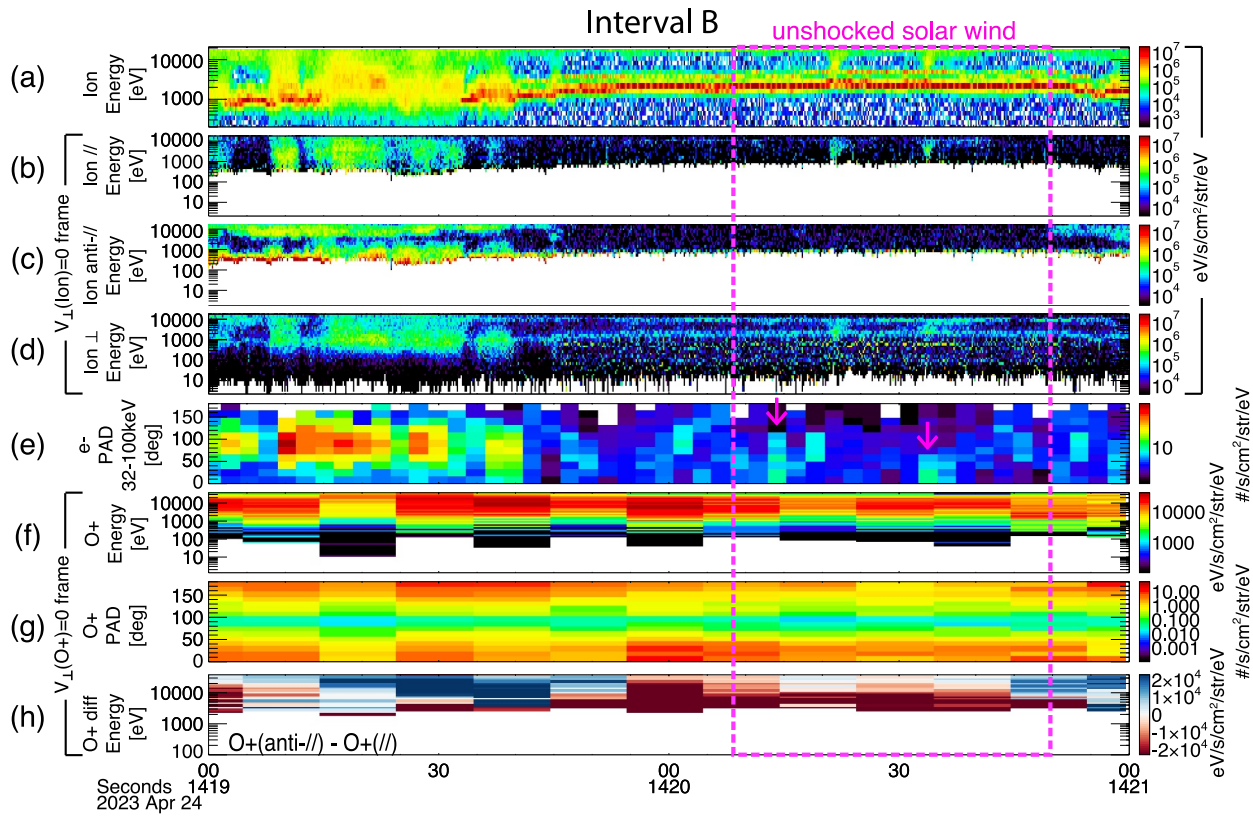

Figure 4. Observations in Interval B (14:19–14:21 UT) from Figure 2: (a) ion energy spectrum, (b) ion parallel (pitch-angle = 0°–45°), (c) anti-parallel (pitch-angle = 135°–180°), and (d) perpendicular (pitch-angle = 67.5°–112.5°) energy flux to the local magnetic field, (e) electron pitch-angle distribution (PAD) with energy of 32–100 keV, (f) O+ omni energy flux, (g) O+ PAD, (h) anti-parallel O+ energy flux (120°–180°) subtracted by parallel energy flux (0°–60°). Panels (b–d) are in the $V_{\perp}(\text{ion}) = 0$ frame. Panels (f–h) are in the $V_{\perp}(O+) = 0$ frame. Magenta dashed boxes highlight the unshocked solar wind interval. Magenta arrows highlight the electron jets.

energetic O+, the flux was mainly distributed between 8 and 20 keV, a narrower energy band than that in the Alfvén wing filaments between 14:05 and 14:24 UT.

The flux tubes consisted of CFLs, shown by the enhancement of energetic electron PAD (Panel f1). The O+ fluxes were primarily within two pitch angle ranges 0°–60° and 120°–180° (Panel h1). This O+ distribution, along with the heated H+ background (Figure 5c1), resembles the newly-formed CFLs during the Alfvén wing state. As shown in Figure 3c, for the newly-formed CFLs (red dashed boxes), fluxes are mainly at 0°–60° and 120°–180°, while earlier-formed CFLs (blue dashed boxes) show significant flux extending to 90°. Figure 5h1 indicates the observed flux tubes are similar to the newly-formed CFLs. This similarity suggests these flux tubes may be relics of newly-formed CFLs from the Alfvén wing state, providing insights into the magnetic structure evolution during the recovery phase.

The flux tubes' thicknesses were slightly larger than or comparable to the O+ gyro-scales. The average perpendicular flow speed ($V_{\perp}(H+)$) from 15:00 to 15:22 UT was about 400 km/s. The timescales of the nine isolated flux tubes were 4, 13, 3, 25, 8, 3, 3, 28, and 17 s. Multiplying these timescales by the perpendicular flow speed gives their thicknesses, 1,600, 5,200, 1,200, 10,000, 3,200, 1,200, 1,200, 11,200, and 6,800 km respectively. The gyroradius of a 20-keV O+ with a 60° pitch angle in a 40-nT field is about 1,800 km. O+ fluxes were observed over a broader region than the flux tubes due to the O+ finite gyroradius. Satellites would observe O+ ions gyrating around the field lines at the flux tube's outermost shell before/after observing the flux tube. The significant parallel or anti-parallel velocity component of these O+ ions suggests that they were prone to loss, especially when the flux tube had a complex configuration comparable to the O+ gyro-scales. For instance, if the flux tube was kinked, O+ ions that were originally executing their helical motion inside the tube might shoot

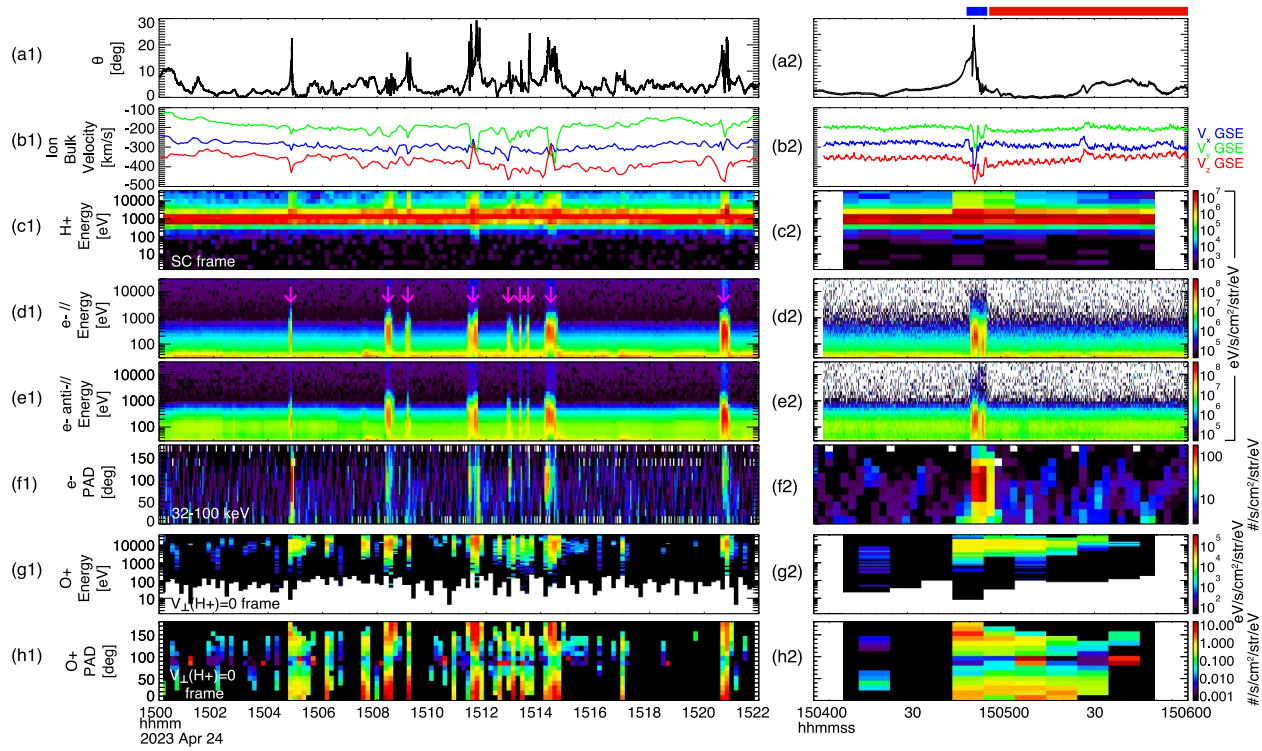

Figure 5. Observations between 15:00 and 15:22 UT: Left column – (a1) deviation angle of magnetic field from the background interplanetary magnetic field (IMF), (b1) ion bulk velocity, (c1) H+ energy fluxes in the spacecraft frame, (d1) parallel and (e1) anti-parallel field-aligned electron energy fluxes, (f1) electron pitch-angle distribution (PAD) with energy of 32–100 keV, (g1) and (h1) O+ energy flux and PAD in the $V_{\perp}(H+) = 0$ frame. Right column – (a2–h2) zoom-in plots of (a1–h1) between 15:04 and 06 UT. Blue and red bars highlight intervals containing closed field lines and IMF, respectively. The background IMF is averaged over 15:00–15:22 UT for (a1) and 15:05:05–15 UT for (a2).

beyond the tube and end up in the solar wind. Similarly, the observed O+ in the solar wind (e.g., between 15:06-08 UT) might also come from other flux tubes not in the MMS path.

A pitch-angle dispersion in anti-parallel O+ flux was observed starting around 15:05 UT in Figure 5h1, seen as a gradual loss of O+ flux in 120°–180°. The exact mechanism for this dispersion is unclear, but the kinked flux tube scenario offers one possible explanation for the asymmetric loss in the PAD. The Panels (a2–h2) show zoom-in results from 15:04 to 06 UT. Intervals with CFLs (blue bar) and IMF (red bar) signatures are determined based on electron signatures in Panels d2–f2. Panel a2 shows the flux tube field deviated from the background IMF by a maximum of 28°. O+ ions could gyrate in a helical motion oscillating between the flux tube and solar wind regions. If the deviation angle between the flux tube and IMF remains the same along the tube, the parallel and anti-parallel O+ fluxes (Panel h2) should show the same variations when MMS cutting through the solar wind after leaving the flux tube. However, if the O+ ions encounter a kink (significant change of deviation angle) on the scale of their gyromotion, they might fail to return to the tube and be lost to the solar wind. Consequently, the parallel and antiparallel O+ fluxes could show different variations if one direction was influenced by a kink before reaching MMS. The observed gradual loss in nearly anti-parallel flux along the MMS path, compared to the relatively unaffected parallel flux, indicates that this mechanism was likely at play.

4. Summary and Conclusion

We study the O+ characteristics during the Alfvén-wing state of the magnetosphere induced by the CME event on 24 Apr 2023, using MMS observations. MMS was located in the dayside pre-noon sector near the southern cusp at (10.7, −7.9, −6.8) R_E in the GSE coordinates. This is the first observation of O+ in Earth's Alfvén wing. Key points are summarized below:

1. The observed O+ characteristics, including bidirectional streaming along newly-formed CFLs and dominant anti-parallel flow on earlier-formed CFLs, have important implications for understanding O+ transport and

trapping during Alfvén wing states, revealing new aspects of heavy ion circulation different from typical storm-time scenarios.

2. The presence of escaping O+ ions, along with energetic protons and electrons in the unshocked solar wind, highlights a potential loss mechanism during the Alfvén wing state. The fate of these escaping O+ ions remains uncertain, as they may either propagate with the MC or return to the magnetosphere. This finding has implications for understanding heavy ion loss processes in Earth's magnetosphere and other planetary magnetospheres and moons experiencing the Alfvén wing state.
3. The O+ pitch-angle dispersion is observed associated with magnetic flux tubes, indicating potential loss to the solar wind. These flux tubes appeared during the recovery phase of the Alfvén wing state, when the solar wind returned to super-Alfvénic speeds (M_A = 1.1–2.0). This suggests a subsequent loss mechanism immediately after the Alfvén wings disappear.

This study also underscores the need for future research to fully elucidate O+ ion transport and energization mechanisms under extreme conditions. Multi-point measurements and global simulations are essential to map the O+ transport pathways from various source regions to the observed location near the cusp region. The O+ characteristics observed in this study, particularly their energy ranges and spatial distributions, provide critical input for future global simulations and multi-point observational studies.

Data Availability Statement

MMS data are publicly available at https://lasp.colorado.edu/mms/sdc/public/. The SPEDAS (Space Physics Environment Data Analysis Software) from http://spedas.org/blog/ has been used for data analysis.

Acknowledgments
HL would like to express gratitude to Dr. Ying Zou for the valuable discussions. This study is supported by the NASA MMS Mission. HL acknowledges partial support from NASA Grant 80NSSC24K0388. HL and HG acknowledge partial support of NSF Grant AGS2247718.

References

Blake, J., Mauk, B., Baker, D., Carranza, P., Clemmons, J., Craft, J., et al. (2016). The Fly's Eye Energetic Particle Spectrometer (FEEPS) sensors for the Magnetospheric Multiscale (MMS) mission. *Space Science Reviews*, *199*(1–4), 309–329. https://doi.org/10.1007/s11214-015-0163-x

Burch, J. L., Torbert, R. B., Phan, T. D., Chen, L. J., Moore, T. E., Ergun, R. E., et al. (2016). Electron-scale measurements of magnetic reconnection in space. *Science*, *352*(6290), aaf2939. https://doi.org/10.1126/science.aaf2939

Burkholder, B. L., Chen, L. J., Fuselier, S., Gershman, D., Schiff, C., Shuster, J., et al. (2022). MMS observations of storm-time magnetopause boundary layers in the vicinity of the Southern cusp. *Geophysical Research Letters*, *49*(24), e2022GL101231. https://doi.org/10.1029/2022gl101231

Burkholder, B. L., Chen, L.-J., Sarantos, M., Gershman, D. J., Argall, M. R., Chen, Y., et al. (2024). Global magnetic reconnection during sustained sub-Alfvénic solar wind driving. *Geophysical Research Letters*, *51*(6), e2024GL108311. https://doi.org/10.1029/2024gl108311

Chané, E., Raeder, J., Saur, J., Neubauer, F. M., Maynard, K. M., & Poedts, S. (2015). Simulations of the Earth's magnetosphere embedded in sub-Alfvénic solar wind on 24 and 25 May 2002. *Journal of Geophysical Research: Space Physics*, *120*(10), 8517–8528. https://doi.org/10.1002/2015ja021515

Chané, E., Saur, J., Neubauer, F. M., Raeder, J., & Poedts, S. (2012). Observational evidence of Alfvén wings at the Earth. *Journal of Geophysical Research*, *117*, A09217. https://doi.org/10.1029/2012JA017628

Chappell, C. R., Huddleston, M. M., Moore, T. E., Giles, B. L., & Delcourt, D. C. (2008). Observations of the warm plasma cloak and an explanation of its formation in the magnetosphere. *Journal of Geophysical Research: Space Physics*, *113*(A9). https://doi.org/10.1029/2007ja012945

Chen, L. J., Gershman, D., Burkholder, B., Chen, Y., Sarantos, M., Jian, L., et al. (2024). Earth's Alfvén wings driven by the April 2023 coronal mass ejection. *Geophysical Research Letters*, *51*(14), e2024GL108894. https://doi.org/10.1029/2024gl108894

Chen, Y., Dong, C., Chen, L. J., Sarantos, M., & Burkholder, B. L. (2024). Interplanetary magnetic field B_y controlled Alfvén wings at Earth during encounter of a coronal mass ejection. *arXiv preprint arXiv:2402.04282*.

Fok, M.-C., Moore, T. E., Brandt, P. C., Delcourt, D. C., Slinker, S. P., & Fedder, J. A. (2006). Impulsive enhancements of oxygen ions during substorms. *Journal of Geophysical Research: Space Physics*, *111*(A10). https://doi.org/10.1029/2006ja011839

Fuselier, S. A. (2020). Ionospheric oxygen ions in the dayside magnetosphere. *Journal of Atmospheric and Solar-Terrestrial Physics*, *210*, 105448. https://doi.org/10.1016/j.jastp.2020.105448

Fuselier, S. A., Anderson, B. J., & Onsager, T. G. (1995). Particle signatures of magnetic topology at the magnetopause: AMPTE/CCE observations. *Journal of Geophysical Research: Space Physics*, *100*(A7), 11805–11821. https://doi.org/10.1029/94ja02811

Fuselier, S. A., Anderson, B. J., & Onsager, T. G. (1997). Electron and ion signatures of field line topology at the low-shear magnetopause. *Journal of Geophysical Research: Space Physics*, *102*(A3), 4847–4863. https://doi.org/10.1029/96ja03635

Fuselier, S. A., Haaland, S., Tenfjord, P., Paschmann, G., Toledo-Redondo, S., Malaspina, D., et al. (2021). High density magnetospheric He+ at the dayside magnetopause and its effect on magnetic reconnection. *Journal of Geophysical Research: Space Physics*, *126*(1), e2020JA028722. https://doi.org/10.1029/2020JA028722

Fuselier, S. A., Kletzing, C. A., Petrinec, S. M., Trattner, K. J., George, D., Bounds, S. R., et al. (2022). Multiple reconnection X-lines at the magnetopause and overlapping cusp ion Injections. *Journal of Geophysical Research: Space Physics*, *127*(5), e2022JA030354. https://doi.org/10.1029/2022ja030354

Fuselier, S. A., Mukherjee, J., Denton, M. H., Petrinec, S. M., Trattner, K. J., Toledo-Redondo, S., et al. (2019). High-density O+ in Earth's outer magnetosphere and its effect on dayside magnetopause magnetic reconnection. *Journal of Geophysical Research: Space Physics*, *124*(12), 10257–10269. https://doi.org/10.1029/2019ja027396

Fuselier, S. A., Trattner, K. J., Petrinec, S. M., Denton, M. H., Toledo-Redondo, S., André, M., et al. (2019). Mass loading the Earth's dayside magnetopause boundary layer and its effect on magnetic reconnection. *Geophysical Research Letters*, *46*(12), 6204–6213. https://doi.org/10.1029/2019gl082384

Gurram, H., Shuster, J. R., Chen, L. J., Hasegawa, H., Denton, R. E., Burkholder, B. L., et al. (2024). Earth's Alfvén wings: Unveiling dynamic variations of field-line topologies with electron distributions. *arXiv preprint arXiv:2409.00247*.

Jordanova, V. K., Ilie, R., & Chen, M. W. (Eds.). (2020). *Ring current investigations: The quest for space weather prediction*. Elsevier.

Kivelson, M. G., Bagenal, F., Kurth, W. S., Neubauer, F. M., Paranicas, C., & Saur, J. (2004). Magnetospheric interactions with satellites. In F. Bagenal, T. E. Dowling, & W. B. McKinnon (Eds.), *Jupiter. The planet, satellites and magnetosphere* (pp. 513–536). Cambridge University Press.

Kivelson, M. G. & Russell, C. T. (Eds.). (1995). *Introduction to space physics*. Cambridge University Press.

Kronberg, E. A., Ashour-Abdalla, M., Dandouras, I., Delcourt, D. C., Grigorenko, E. E., Kistler, L. M., et al. (2014). Circulation of heavy ions and their dynamical effects in the magnetosphere: Recent observations and models. *Space Science Reviews*, *184*(1–4), 173–235. https://doi.org/10.1007/s11214-014-0104-0

Lavraud, B., & Borovsky, J. E. (2008). Altered solar wind-magnetosphere interaction at low Mach numbers: Coronal mass ejections. *Journal of Geophysical Research: Space Physics*, *113*(A9). https://doi.org/10.1029/2008ja013192

Liao, J., Kistler, L. M., Mouikis, C. G., Klecker, B., & Dandouras, I. (2015). Acceleration of O+ from the cusp to the plasma sheet. *Journal of Geophysical Research: Space Physics*, *120*(2), 1022–1034. https://doi.org/10.1002/2014ja020341

Lugaz, N., Farrugia, C. J., Huang, C. L., Winslow, R. M., Spence, H. E., & Schwadron, N. A. (2016). Earth's magnetosphere and outer radiation belt under sub-Alfvénic solar wind. *Nature Communications*, *7*(1), 13001. https://doi.org/10.1038/ncomms13001

Möbius, E., Hovestadt, D., Klecker, B., Scholer, M., Ipavich, F. M., Carlson, C. W., & Lin, R. P. (1986). A burst of energetic O+ ions during an upstream particle event. *Geophysical Research Letters*, *13*(13), 1372–1375. https://doi.org/10.1029/gl013i013p01372

Neubauer, F. M. (1998). The sub-Alfvénic interaction of the Galilean satellites with the Jovian magnetosphere. *Journal of Geophysical Research*, *103*(E9), 19843–19866. https://doi.org/10.1029/97JE03370

Pollock, C., Moore, T., Jacques, A., Burch, J., Gliese, U., Saito, Y., et al. (2016). Fast plasma investigation for magnetospheric multiscale. *Space Science Reviews*, *199*(1–4), 331–406. https://doi.org/10.1007/s11214-016-0245-4

Ridley, A. J. (2007). Alfvén wings at Earth's magnetosphere under strong interplanetary magnetic fields. In *Annales geophysicae, annales geophysicae* (Vol. 25(2), pp. 533–542). Copernicus Publications. https://doi.org/10.5194/angeo-25-533-2007

Russell, C. T., Anderson, B. J., Baumjohann, W., Bromund, K. R., Dearborn, D., Fischer, D., et al. (2014). The magnetospheric Multiscale magnetometers. *Space Science Reviews*, *199*(1–4), 189–256. https://doi.org/10.1007/s11214-014-0057-3

Saur, J., Grambusch, T., Duling, S., Neubauer, F. M., & Simon, S. (2013). Magnetic energy fluxes in sub-Alfvénic planet star and moon planet interactions. *Astronomy & Astrophysics*, *552*, A119. https://doi.org/10.1051/0004-6361/201118179

Young, D. T., Burch, J. L., Gomez, R. G., De Los Santos, A., Miller, G. P., Wilson, P. I. V., et al. (2016). Hot plasma composition analyzer for the magnetospheric multiscale mission. *Space Science Reviews*, *199*(1–4), 407–470. https://doi.org/10.1007/s11214-014-0119-6